Article

Embedded Cyber-Physical System for Physiological Control of Ventricular Assist Devices

Bruno Jesus dos Santos[1,2,3,*] , **Tarcisio Fernandes Leão[1,4]** , **Marcelo Barboza Silva[1]**, **Evandro Drigo da Silva[1] and Eduardo Guy Perpétuo Bock[1]**

[1]Bioengineering Laboratory, Department of Mechanical and Electrical Engineering, Federal Institute of São Paulo, São Paulo, Brazil
[2]Department of Information Technology, University São Judas Tadeu, São Paulo, Brazil
[3]Department of Biomedical Engineering, Polythecnic School of Engineering, University of São Paulo, São Paulo, Brazil
[4]Department of Bioengineering, Institute Dante Pazzanese of Cardiology, São Paulo, Brazil
E-mail: brunojsantos@usp.br

Abstract: Ventricular Assist Devices (VADs) play a crucial role in both bridging to transplantation and serving as destination therapy for congestive heart failure (CHF) management. This study aims to address the limitations of existing control strategies for VADs, specifically their inability to adapt automatically to hemodynamic changes. It proposes a novel embedded cyber-physical system (CPS) based on real-time data processing, reconfigurable architecture, and communication protocols aligned with Health 4.0 concepts to enhance physiological control over VADs (PC-VAD). The research employs a multi-objective PC-VAD approach within a hybrid cardiovascular simulator. An embedded CPS is introduced to overcome challenges related to differences in controller characteristics between computers and embedded systems. The study assesses the performance of the embedded CPS by comparing it with a computer-based control system. The embedded CPS demonstrates outcomes comparable to the computer-based control system, maintaining mean arterial pressure and cardiac output at physiological levels. Even in the face of variations in ejection fraction, the embedded CPS dynamically adjusts the pump's rotational speed based on simulated clinical conditions. Notably, there is no aortic reflux to the ventricle through the VAD during testing. These findings affirm the satisfactory control performance of the embedded CPS in regulating VADs. The study concludes that the embedded CPS effectively addresses the limitations of current VAD control strategies, exhibiting control performance comparable to computer-based systems. However, further experimentation and in vivo studies are necessary to validate and ensure its applicability in real-world scenarios.

Keywords: ventricular assist device, physiological control, intelligent embedded system, cyber-physical system

1. Introduction

Heart Failure (HF) is a major global health problem, with Congestive HF (CHF) being the most debilitating stage, characterized by the inability of the heart to pump enough blood to maintain a healthy life [1]. While heart transplantation remains the gold standard for treating end-stage CHF, the limited number of available donors and potential contraindications limit its effectiveness [2].

Left and Right Ventricular Assist Devices (RVAD and LVAD) are used to prevent mortality in patients awaiting heart transplantation (bridge to transplant; BTT) and as destination therapy (DT) for those ineligible for transplantation [3]. Although each technological advance has been successful, adverse events continue to

complicate the long-term management of LVAD patients. However, with the current generation, their incidence has been significantly reduced [4].

Continuous-flow LVADs (cfLVADs) can experience challenges related to balancing the assist flow with changes in posture and physical activity, such as insufficient pumping with/without reflux and excessive pumping with/without ventricular suction. Commercial cfLVAD controllers control the constant blood flow pumping rate, and clinicians adjust the flow when they detect a new need for assistance during periodic visits [5]. The inability of devices to automatically respond to changes in demand can significantly impact the quality of life for these patients. To mitigate this, physiological control of the LVADs (PC-LVADs) has been proposed as a system that facilitates automatic speed setpoint adjustments in rapid response to demand and circulatory conditions [6]. PC-LVADs have been developed with different controllers and monitoring strategies [7]. Despite promising outcomes, the adoption of these PC-LVAD strategies on computers encounters limitations stemming from substantial disparities and inherent constraints characteristic of embedded systems, such as PC-LVAD strategies developed utilizing the computer as a controller.

This study investigates the migration of PC-LVAD functionality into an intelligent embedded system that integrates real-time data processing, reconfigurable architecture, and communication protocols. It explores the application of the system as an embedded Cyber-Physical System (CPS) in healthcare, harmonizing computational and physical elements. The characteristics and behavior of the system are compared between a conventional computer and an embedded CPS. The PC-LVAD is modularized, validated in a simulated loop, and integrated into an architecture. Its automatic adjustment of LVAD speed within a hybrid cardiovascular system (HCS) simulator is evaluated.

To the best of our knowledge, the implementation of PC-LVADs within an embedded HCS remains unexplored and has the potential to improve LVAD control and thereby contribute to improved patient outcomes. Therefore, it is imperative to explore the development of embedded systems tailored for PC-LVADs.

The exposition begins with an introduction in Section 1, followed by a review of related works concerning PC-LVADs studies analysis in Section 2, followed by an in-depth presentation of the embedded CPS development in Section 3. This section also evaluates the feasibility and performance of the proposed system. Section 4 outlines the findings discussed in Section 5. The exposition concludes with a summary in Section 6.

2. Related Works

Researchers have developed several PC-LVADs with controllers and monitoring strategies [7]. To simplify the analysis, one can categorize these studies into four main classes [8]: (i) Preload-based controllers employ pressure sensors to adjust the LVAD speed in response to variations in ventricular preload, aiming to emulate the Frank-Starling mechanism; (ii) Afterload-based controllers utilize algorithms to determine the LVAD speed based on the pressure difference between the inlet and outlet, seeking to maintain a constant pressure difference between the left ventricle and the aorta; (iii) Heart rate-based controllers, which regulate the LVAD speed according to heart rate, incorporating physiological responses during activities such as exercise; and (iv) Multi-objective controllers aim to simultaneously optimize physiological parameters, including aortic pulsatility, aortic valve opening, ventricular load, and heart rate, ensuring safe and efficient LVAD operation.

The research conducted by Waters et al. [9] introduces an LVAD control strategy that utilizes a Proportional-Integral (PI) gain algorithm. This strategy aims to maintain a reference differential pressure despite changes in native heart function. The relationship between motor current, voltage, and counter electromotive force (emf) for blood flow and pressure through the LVAD is harnessed to estimate LV pressure and control motor rotation speed.

In a related endeavor, Endo et al. [10] investigated a two-stage control strategy for biventricular assist devices (BiVAD). Their approach is distinctive for not relying on sensors to detect ventricular collapse. The Current Amplitude Index (CAI) formula is applied to calculate the current waveform of each BiVAD motor.

Concurrently, Ohuchi et al. [11] propose a control strategy that determines the target pump rotation to minimize harmful effects and assess ventricular function. Leveraging the relationship between native heart rate and cardiac output and analyzing the motor current waveform is involved in quantifying waveform deformation and ascertaining suction effects.

Bullister et al. [12] introduced a hierarchical LVAD control strategy, where the speed setting value is regulated using pump inlet pressure as the primary independent variable and pump outlet pressure as the

secondary dependent variable. This strategy incorporates two levels of control: (i) Level 1 control maintains left ventricular diastolic pressure (LVEDP) filling pressure within a physician-programmable range, incrementally pumping all incoming blood from the LV; (ii) Level 2 control ensures the mean pump outlet pressure remains at a target value during high levels of ventricular pulsation, such as during exercise, using heart rate as a physiological indicator. Regulating the sympathetic nervous system of the circulatory system during exercise or stress is essential for this process.

Boston et al. [13] proposed an LVAD control strategy that determines the reference speed through ideal, heuristic, or standard algorithms. An intelligent control supervisor monitors patient activity and estimated model parameters, selects the control algorithm, and compares previous system history to detect hardware failures or changes in the patient. However, the standard control mode may result in low cardiac output and adverse regurgitant flow through the pump circuit.

Vollkron et al. [14] developed a physiological control system for rotary LVADs that monitors venous return, adapts pump performance with periodic speed variations, and compares available returns to required perfusion levels to establish the desired flow. This study stands as a landmark in the field, being the only rotary LVAD physiological control system that has undergone clinical evaluation [15], highlighting the benefits of physiological control for patients with rotary LVADs.

Giridharan et al. [16] proposed an LVAD control strategy that employs an algorithm to define the speed setting value based on the estimated differential pressure (ΔP) between the pump inlet and outlet pressure. The aim is to maintain a constant mean reference pressure difference between the LV and the aorta by manipulating the pump speed and motor current.

Wu et al. [17] proposed an optimal adaptive LVAD controller composed of an adaptive parameter estimation algorithm, an adaptive state observer, and an optimal PI controller. This controller aims to control the estimated aortic pressure and meet the patient's physiological needs by tracking an updated reference signal through a non-linear function of the pump pressure gradient.

Choi et al. [18] introduced an LVAD control strategy that utilizes a fuzzy logic algorithm to define the speed setting value and obtain an appropriate pulsatility ratio that meets the physiological demands of the patient while avoiding adverse conditions.

Gwak [19] proposed an LVAD control strategy that utilizes an extreme search control (ESC) algorithm to define the demand-based speed setting value based only on estimated pump flow information corresponding to the maximum cardiac output without the risk of suction.

The study conducted by Arndt et al. [20] proposes an LVAD control strategy with two operational modes (total and partial assistance) based on regulating the LV filling pressure or volume through the differential pressure signal (dP) pulsatility index (PI) between the inlet and outlet of the LVAD.

Stevens et al. [21] introduced a master/slave system for dual LVADs in biventricular support. The master controller functions as a Frank-Starling type controller, establishing the flow rate as a function of the end-diastolic pressure of the LV (EDPLV). Simultaneously, the slave controller maintains a linear relationship with each LVAD equipped with two pressure sensors and one flow sensor. Additionally, Stephens et al. [22] report on a Starling-like physiological controller with sigmoidal control lines, providing high preload sensitivity at moderate to low preloads and decreasing to prevent over-pumping at high preloads. Including a physiological response path mimicking the venous return curve, combined with the Starling curve, automatically balances pulmonary and systemic circulations. The control feedback relies on minimum diastolic pressures of the LV and right ventricle (RV).

Cysyk et al. [23] implemented a bang-bang control system to regulate the pump speed based on changes in the peak-to-peak input pressure signal (Pppk; measured with a pressure sensor) calculated over an average of N cycles with the Pppk set point. Subsequently, Cysyk et al. [24] utilized the reference of the Pressure-Volume Area (PVA; pressure measured by sensor and volume detected by conductance electrodes) to adjust the pump speed automatically.

In the study by Petrou et al. [25], a physiological controller for a cfVAD is proposed based on the LV pressure recorded at the inlet cannula. This controller, which requires only a pressure sensor, utilizes the LV systolic pressure (SP) as an indicator to determine variable perfusion needs. The algorithm for extracting SP from the pump inlet pressure signal, used to adjust the speed, demonstrated robust behavior. A sensitivity analysis of the controller's parameters was conducted to identify their limits and influence on circulation. The proposed SP controller exhibited satisfactory performance for different values of LV contractility and for a simulated deviation of the pressure sensor, eliminating events of over and under pumping.

Petrou et al. [26] present a new multi-objective physiological control system for LVADs, which employs pump inlet pressure to adapt pump flow to meet physiological requirements. It aims to increase aortic pulse pressure, ensure aortic valve opening, provide LV pre and afterload information, and monitor heart rate. The system ensures safe operation without suction, LV overload, or backflow events. In vitro assays demonstrate its potential for a safe physiological response with a reduced risk of myocardial atrophy and important hemodynamic indices for patient monitoring.

Fetanat et al. [27] proposed a novel real-time deep convolutional neural network (CNN) to estimate preload based on LVAD flow. This proposition aims to develop a sensorless adaptive physiological control system for LVADs, demonstrating feasibility and accuracy in evaluating preload. It maintains patient conditions within safe physiological ranges and prevents ventricular suction and pulmonary congestion.

Leão et al. [28] proposed a multi-objective physiological control (MOPC) for LVADs that optimizes the device-body interaction and operates with the physiological control system. The MOPC comprises three layers: (i) Proportional-Integral (PI) control, (ii) flow control based on physiological parameters, and (iii) automatic control using fuzzy logic. The MOPC speed operates harmoniously within the physiological control system based on the following input variables of the fuzzy logic: average heart rate (aHR), mean arterial pressure (MAP), minimum pump flow (mF), patient activity level (PA), and clinician-defined patient profile (PP). The automatic control adjusts the flow rate of the second layer, which, in turn, modifies the pump speed.

Each PC-LVAD presents specific advantages, alongside challenges and complexities. The Multi-Objective Control system epitomizes sophistication. Assessing the applicability of these strategies in specific clinical contexts necessitates a detailed analysis of each approach's characteristics and specific requirements [29].

Implementation of PC-LVAD strategies in embedded systems could leverage processing power and sensor integration to dynamically adapt LVAD performance to physiological patient demands. For example, the approach proposed by Vollkron et al. [14] using a physiological control system for rotating LVADs could be implemented using microcontrollers or system-on-chip (SoC) systems supporting multiple pressure and flow sensors. This would allow monitoring of venous return, adjustment of pump performance with periodic speed variations, and comparison of available return with required perfusion levels to determine desired flow, all in real-time and autonomously. In addition, strategies such as those described by Petrou et al. [26], using a pressure sensor on the LVAD inlet cannula and systolic pressure detection algorithms, could be adapted in an embedded system using signal processing and embedded control techniques to regulate pump speed based on real-time pressure measurements, mimicking the Frank-Starling mechanism. Integrating these approaches into an embedded system would require careful consideration of power consumption, system latency, and robustness to ensure an adaptive and reliable response to changes in patient physiological conditions, which is critical to improving patient hemodynamic stability while maintaining device safety and efficacy.

An embedded system, often limited and inflexible, is portable and designed for specific applications. Fontana et al. [30] presented an innovative solution in the form of a wearable and reconfigurable system designed to interface with sensors in cfLVADs within a comprehensive monitoring and self-regulation framework. This pioneering platform integrates wireless control capabilities and a wearable system interface, providing patients with newfound freedom and comfort while ensuring seamless integration into their daily lives. In addition, the anticipated integration of this controller with the SensorART platform promises to improve both patient outcomes and physician workflow efficiency [31]. However, the potential to further enhance PC-LVADs by incorporating additional artificial intelligence (AI) algorithms warrants significant attention [27,28]. These advanced algorithms could leverage the wealth of data generated by estimators and sensors, enabling more precise and responsive control mechanisms within a supervisory system framework. By harnessing the power of AI, PC-LVADs could evolve into truly adaptive and intelligent systems capable of continuously optimizing their performance to meet the unique needs and preferences of each patient. In addition, those that use field-programmable gate arrays (FPGA) are reprogrammable and exhibit computational parallelism, making them suitable for PC-LVAD control. Integrating a hybrid embedded system with FPGA architecture and real-time operating system (RTOS) processing requires efficient coordination to take advantage of both technologies. Evolving embedded technology enables the fusion of FPGA architecture with an RTOS processor in a SoC environment. The resulting design can encapsulate intellectual property in a single board or integrated module.

The study conducted by Fass & Gechter [32] introduces a novel isomorphic framework designed for modeling both natural and artificial systems, to redefine the concept of human-in-the-loop (HITL) systems. This innovative framework categorizes system dimensions into three distinct components: structural elements,

shapes/forms, and dynamics. By establishing relationships among these variables, the framework proposes three specification plans: architecture, behavior, and evolution.

The architecture plan focuses on defining the structural elements and shapes/forms that comprise the system, providing insight into its fundamental composition and organization. The Behavior Plan delves into the system's analytic functions, describing how shapes/forms interact with dynamics to produce observable behaviors. Finally, the evolution plan explores the physical, logical, and biological interactions that drive the system's evolution and adaptation over time.

In line with this paradigm, our research group has introduced a PC-LVAD within a Health 4.0 framework. This PC-LVAD, running on an embedded system, represents a practical implementation model for intelligent controllers within this emerging line of research [33]. By integrating the principles of the isomorphic framework with the capabilities of Health 4.0 technologies, our work aims to improve the functionality and adaptability of mechanical circulatory support systems, ultimately improving patient outcomes and advancing the field of personalized medicine.

3. Methods

3.1 *Proposal*

The proposed controller for PC-LVADs is an embedded CPS referred to as an Intelligent Embedded System (IES). This terminology is assigned due to its distinctive features, including reconfigurable architecture and real-time processing tailored for PC-LVADs.

The MOPC method proposed by Leão et al. [28], has been selected for integration into the IES. It optimizes the device-body interaction of LVADs and works with the natural physiological control system. The MOPC includes PI control, flow control based on physiological parameters, and automatic control using fuzzy logic. The MOPC speed works harmoniously within the physiological control system based on aHR, MAP, mF, PA, and PP. The automatic controller adjusts the flow rate, which changes the pump speed. The MOPC method adapts flow adjustments to the physiological subtleties of the patient. It was selected for the IES because of its prior development and comprehensive architecture, which facilitates testing and evaluation for migration to an embedded system. The effectiveness of MOPC operations is demonstrated by their congruence with physiological parameters in various CHF scenarios [28].

The MOPC was implemented in the IES through a convergence of development tools, including LabVIEW® FPGA and RT (Version 2018, National Instruments, Austin, USA), Quartus II® EDA (Version 9, Altera, San Jose, USA), and MATLAB® (R2018b, MathWorks, Natick, USA). The LabVIEW development environment provides a familiar and efficient platform for embedded system programming, enabling rapid control algorithm development. This makes it easy to implement complex control strategies to meet the physiological needs of the patient.

To ensure the correct operation of the MOPC, look-up tables (LUTs) are created to control the estimators of each LVAD motor. Hydrodynamic testing determines the LUT, establishes a correspondence between velocity and current with flow and differential pressure, and maps it to a three-dimensional surface. The effect of viscosity on LUT formation is suitable for operation within a specified range, as patients use medications to control hematocrit and maintain density within a narrow operating range. Leao and Andrade (No. BR1020160068363/2016) have patented this technique.

During the conceptual phase of the controller design, the IES was implemented in the dedicated PXI® development platform with the 8840 and 7851 modules (National Instruments, Austin, USA). PXI is a modular instrumentation platform that provides high performance and flexibility for a wide range of applications. By combining the processing power of a computer with the versatility of modular instruments, PXI is well-suited for applications that require fast sampling rates, real-time signal processing, and advanced I/O capabilities.

During the controller design evaluation, the IES was implemented on the MyRIO® development board (National Instruments, Austin, USA). The MyRIO provides a compact and integrated solution for medical applications, well suited for environments with limited space and reliability requirements. Its rugged design ensures operational stability under adverse conditions, making it suitable for critical systems such as PC-LVADs. In terms of design features, the MyRIO includes input and output interfaces that are critical for PC-LVADs,

including analog inputs for sensor connection and PWM outputs for pump speed adjustment. In addition, its wireless communication capability and Ethernet enable integration with other monitoring and control systems.

The architectural framework of the EIS, shown in Figure 1, illustrates its seamless integration into the power controller structure. Key components include:

- Data Processing Core: At the core of the EIS resides a processing unit responsible for handling data about actuation systems. It oversees data conversion via the Digital-to-Analog (D/A) converter within the power controller and ingests data through the Analog-to-Digital (A/D) converter linked to transducers.
- Memory Management Unit (MMU): The EIS incorporates an MMU intricately linked to primary memory. Serving as a computational hub, it executes intricate algorithms and manages conditional variables in response to real-world stimuli.
- Communication Interface: A vital element of the EIS is its radio interface, facilitating bidirectional data exchange with external modules. It also enables remote access to a graphical interface for monitoring and control purposes.
- Power Supply: The EIS draws power from a battery source, supplying the requisite energy for its operation, as well as for the embedded system, power controller, and associated actuation systems.
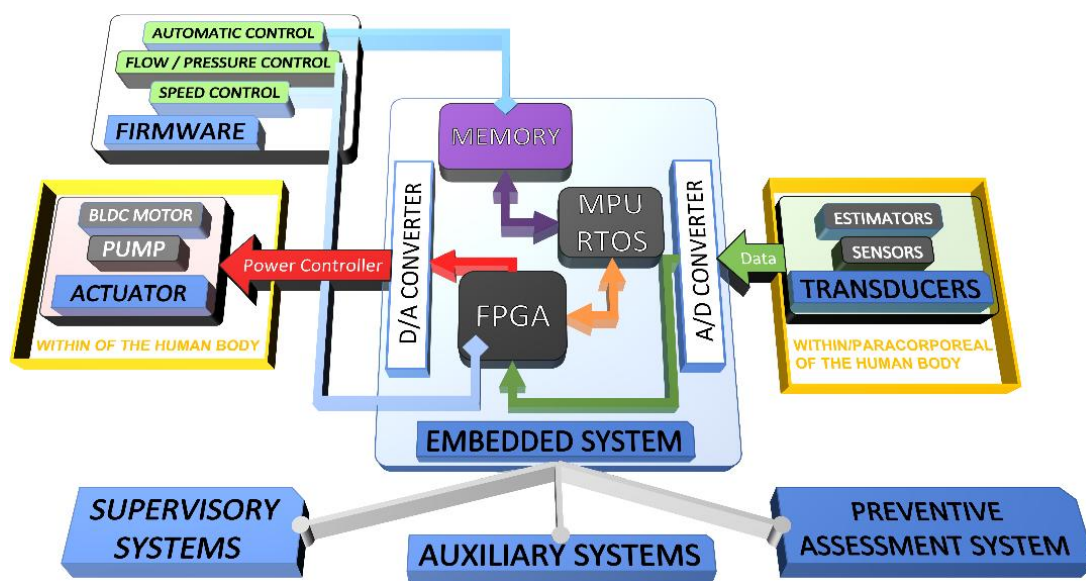

Figure 1. Visual representation of Intelligent Embedded System (IES) architecture integration into the power controller.

The implementation of the EIS comprises various interconnected elements, which can be categorized into four main categories:

1. Control Elements:

- Firmware: The embedded system firmware was developed in high-level LabVIEW programming language and stored in flash memory. The code implements control algorithms, communication interfaces, and system resource management.
- MPU: The microprocessor utilized in the system includes an Intel Core i7 dual-core 2.6 GHz processor for the EIS in PXI 8840 and a 2 GHz ARM Cortex-A9 dual-core for the EIS in MyRio.
- RTOS: The real-time operating system employed is NI Linux Real-Time, ensuring adherence to critical deadlines for system operations.
- Monitoring: The system utilizes estimators from the original MOPC proposal to monitor control variables.

2. Actuation Elements:

- Actuator: The system employs a BLDC motor driven by a 50/4 EC-S electronic system (Maxon, Sachseln, Switzerland), configured using ESCON Studio software (V.18, Maxon, Sachseln, Switzerland), to control motor current.

- FPGA: A Virtex-5 LX30-O FPGA (for EIS in PXI 7851) and Xilinx Z-7010 FPGA (for EIS in MyRio) are utilized to implement the motor control layer.
- Data acquisition: The IES topology involves parallel processing of data acquisition, encompassing instantaneous values (raw and with digital filtering), average values (tuned within 1 second and one complete cycle), and actuation commands associated with a specialized power control system. The implementation adhered to the MOPC processing time. It queued 500 samples of voltage differential at a 5 kHz sampling rate for 0.1 s to feed the pump pressure differential and flow estimators, averaging 50 samples. It queued 2000 samples of voltage differential at a 0.5 kHz sampling rate for 4 s to feed the patient's heart rate estimator, averaging ten samples. A complete cycle of physiological control tuning took 5 seconds.

3. Interface Elements:

- Memory: The system uses flash memory to store firmware and RAM to store temporary data.
- Display and Keyboard: A virtual graphical interface is employed to present system state information to the user and allow user configuration and interaction.

4. Safety and Monitoring Elements:

- Supervision Systems: The system features a supervision system that monitors system temperature, current, and voltage.
- Preventive Evaluation System: A preventive evaluation system is integrated, conducting predictive analyses to identify potential failures and prevent their occurrence.

3.2 *In Vitro Validation*

The feasibility and performance of the embedded CPS will be evaluated through two in vitro tests: (i) "Mock Loop System Tests" for a detailed analysis of the CPS performance in a controlled context, and (ii) "Hybrid Cardiovascular Simulator Tests" to reproduce the complex interactions between the embedded CPS and the dynamics of the cardiovascular system. The goal is to assess the symmetry of the CPS, improve its adaptability and effectiveness in dynamic environments, and ensure seamless integration and optimal performance in real-world applications.

3.2.1. Mock Loop System Tests

The performance evaluation was conducted using a previously documented mock loop system [34] with a prototype LVAD (VAD-MLS) as shown in Figure 2. The system includes a 5-liter acrylic reservoir and 3/8" silicone tubing connected to the VAD prototype. The VAD-MLS control program, developed in LabVIEW® (National Instruments, Austin, USA), runs on a platform (PXIe-8840) with signal modules (NI PXIe-6361 and NI PXI-4022). The manipulated variable is the motor speed (rpm), controlled by an Escon 50/4 EC-S power controller (Maxon Motor, Sachseln, Switzerland). The controlled variable is the VAD flow (L/min), measured by an HT-110 flow transducer (Transonic Systems, Ithaca, USA). Process data including pressure differential (mmHg), current (mA), voltage (V), and motor speed feedback (rpm) are monitored.

The VAD-MLS system integrated with a prototype LVAD underwent three tests using MOPC-PC and MOPC-IES controls. Test 1 validated the effectiveness of the motor speed values for first-tier MOPC control. Test 2 compared the resulting flow, differential pressure, and heart rate values from MOPC-PC estimators and those developed in MOPC-IES. Test 3 compared the results from Matlab® Fuzzy Logic Designer (MOPC-PC) and the fuzzy logic results executed in MOPC-IES. The project used experimental study models with a significance level of 0.05 (5%, $\alpha = 0.05$), and the data were statistically processed using the MATLAB® Statistics Toolbox program.
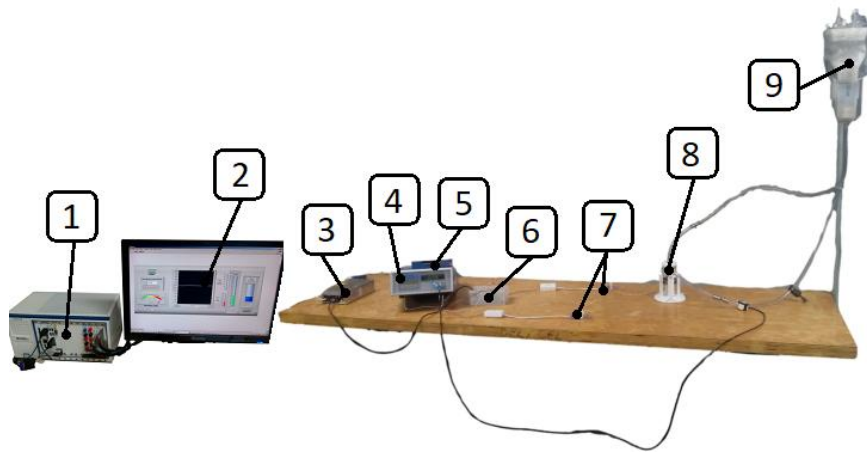
Figure 2. Mock loop system assembled with LVAD prototype. Subtitle: 1- PXIe-8840; 2- Supervisory system; 3- Driver power supply; 4- HT-110 flowmeter; 5- DAQ data acquisition and actuation; 6- Escon 50/4 EC-S driver; 7- Transducers TruWave; 8- VAD prototype; and 9- Reservoir.

3.2.2. Hybrid Cardiovascular Simulator Tests

The HCS was paired with a prototype apical aortic blood pump (AABP) for in vitro evaluation of the MOPC. The AABP, a ceramic-bearing centrifugal blood pump, is designed for long-term circulatory support as an implantable LVAD [35].

The HCS was used to evaluate the MOPC under CHF conditions. The HCS, which consists of computational and physical components, simulates the connection of an LVAD to the cardiovascular system. The computational component emulates the right heart function, while the physical component replicates the left heart and systemic circulation. The HCS has adjustable parameters such as LV contractility, heart rate (HR), and systemic vascular resistance (SVR), and monitors parameters such as LVEF, MAP, AP, intraventricular pressure, SVR, HR, and CO [36].

To evaluate the comprehensive implementation of the MOPC in the IES, referred to as MOPC-IES, two experiments were conducted within the HCS (Figure 3). The purpose of these experiments was to compare the results with those previously obtained using the MOPC-PC within the same simulator. HCS Test 1 evaluated the ability to maintain engine speed during variations in pump resistance with LVEF varied at 15%, 25%, and 35%. HCS Test 2 assessed the response to LVEF variations during recovery of cardiac function, with initial LVEF conditions set at 30%, simulating improvement (LVEF = 40%) or deterioration (LVEF = 15%). PP was adjusted based on LVEF during the simulations, and AP was averaged.
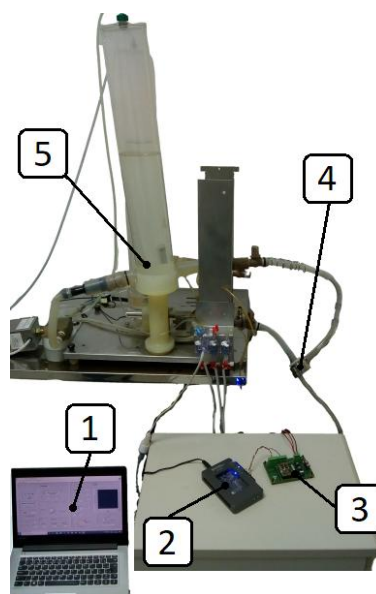

Figure 3. In vitro evaluations of Intelligent Embedded System (IES) in the Hybrid cardiovascular simulator (HCS). Subtitle. 1- IES remote access; 2- IES; 3- Power Controller; 4 - VAD Prototype; 5- left Heart of the HCS.

4. Results

4.1 Mock Loop System Tests

In VAD-MLS Test 1, which evaluated the closed-loop proportional-integral (PI) control of the BLDC motor speed, the mean errors (%) between MOPC-PC and MOPC-IES were comparable (0.60 ± 0.1%), and this similarity was statistically significant (p = 0.986; α = 0.05). The comparison between the actual speed values (measured by the tachometer) and the estimated speed values (measured by the data acquisition system) is shown in Figure 4 for both the conventional computer with DAQ architecture (MOPC-PC, "diamond") and the EIS (MOPC-EIS, "x") equipped with closed-loop PI control of the BLDC motor speed. This graph shows the error rate as a function of the reference speed for motor control and shows two curves, one for MOPC-PC and the other for MOPC-EIS. In the MOPC-PC graph, the error rate varies with the reference speed, starting at about 0.3% for a reference speed of 5000 rpm and decreasing to about 0.1% for a reference speed of 60000 rpm. The error curve shows a relatively smooth behavior, with an increase in rate in the range up to 10000 rpm and again around 40000 rpm. Conversely, in the MOPC-EIS graph, the error rate also varies with reference speed, but to a greater extent than in the MOPC-PC graph for values below 40000 rpm. The error rate starts at about 0.15% for a reference speed of 5000 rpm and decreases to 0.02% for a reference speed of 60,000 rpm. The curve is very similar to the MOPC-PC but shows an increase in error rate before the 20000 rpm speed range. The disturbance test did not show any overshoot or steady state time changes in the motor control. This performance can be attributed to the proper calibration of the PI controller.
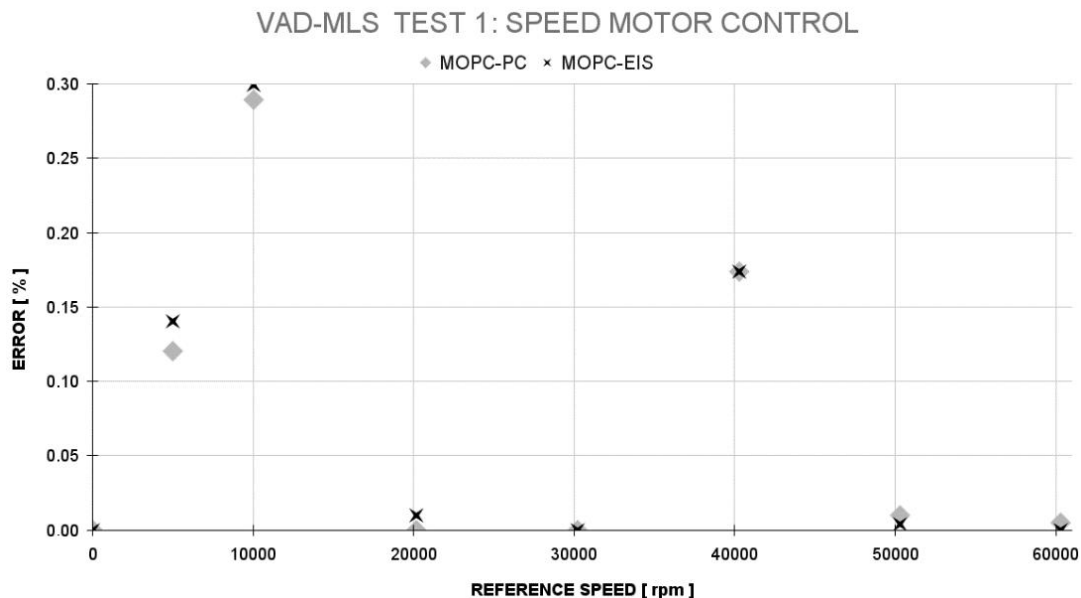

Figure 4. Graph depicting the error relationship between the measured data and the reference value with the motor speed control of the MOPC running on the PC and the IES during the VAD-MLS Test 1.

The VAD-MLS test 2 on the estimators produced estimates with mean errors of (i) 2.6 ± 0.7% (p = 0.94; α = 0.05) for flow, (ii) 0.34 ± 0.1% (p = 0.8; α = 0.05) for differential pressure, and (iii) 0.72 ± 0.7% (p = 0.91; α = 0.05) for heart rate. These mean errors are consistent with those obtained by MOPC estimators on the PC (Leão et al.2020).

Figure 5 compares the flow and differential pressure estimator values obtained by the MOPC-PC architecture and MOPC-IES with a percentage error within the measurement range of 8 L/min and 150 mmHg, respectively. The flow estimator graph in Figure 5 shows 20 data points for each method, MOPC-PC ("diamond") and MOPC-EIS ("x"), comparing their flow estimation results to the reference ("reference flow") within the 5% error range. Regarding the MOPC-PC accuracy: (i) the majority of points (16, 80%) fall within the 5% error range (indicated by dashed lines on the graph); (ii) 4 points (20%) show errors above 5%, with the largest error being approximately 11%; (iii) 9 points (45%) show errors below 2%, with the smallest error being close to 0%. Conversely, for the MOPC-EIS accuracy: (i) most points (15, 75%) fall within the 5% error range; (ii) 5 (25%) points have errors above 5%, with the largest error around 12%; and (iii) 8 points (40%) have errors

below 2%, with the smallest error near 0%. The differential pressure estimation graph in Figure 5 shows 30 data points for each method, MOPC-PC ("diamond") and MOPC-EIS ("x"), comparing their differential pressure estimation results to the reference ("reference pressure") within a 5% error range. For MOPC-PC accuracy: (i) 26 points (86.7%) fall within the 5% error range; (ii) 4 points (13.3%) have errors above 5%, with the largest error being 8%; (iii) 23 points (76.7%) have errors below 2%, with the smallest error being 0%. Conversely, for the precision of the MOPC-EIS: (i) 28 points (93.3%) are within the 5% error range; (ii) 2 points (0.1%) have errors above 5%, with the largest error at 7%; and (iii) 22 points (73.3%) have errors below 2%, with the smallest error at 0%.
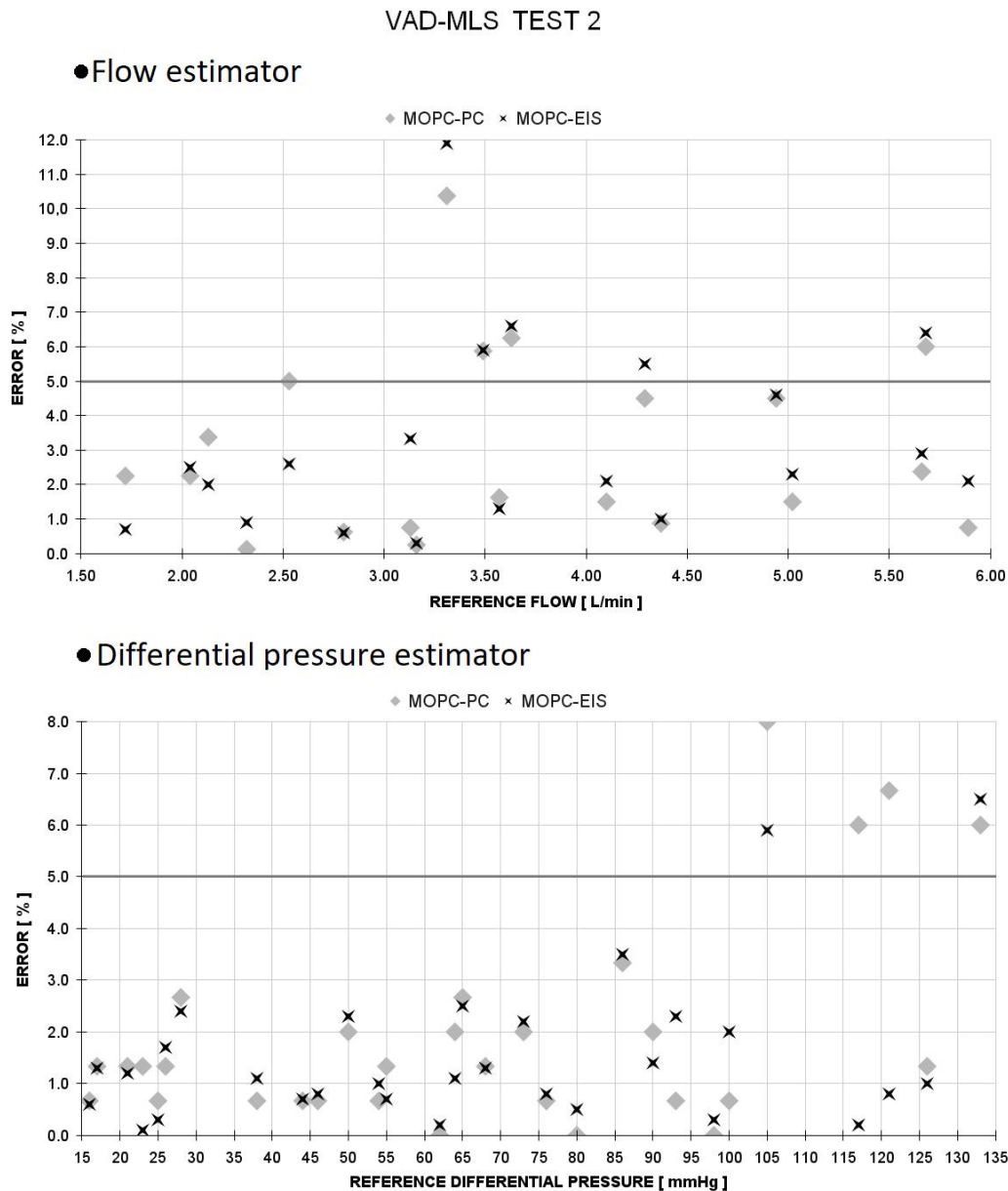

Figure 5. Graph depicting the error relationship between the measured data compared to the reference value with the flow and differential pressure estimator between the MOPC running on the PC and the IES during the VAD-MLS Test 2.

Analysis of the flow range (1.5–6 L/min) shows clear differences between the MOPC-PC and MOPC-EIS methods. MOPC-PC, represented by diamonds, shows good agreement with the reference over all ranges, with most points showing errors below 5%. In the 1.5 to 3 L/min range, all points have errors below 5%, indicating consistent accuracy. However, as the flow increases, the dispersion of the points also increases, with some points showing more significant errors, particularly in the 3.5 L/min and 5.5 L/min ranges. On the other hand, MOPC-EIS, represented by "X", shows fewer points and greater data scatter across all pressure ranges. Although it also shows good agreement with the reference, with most points having errors below 5%, the

dispersion of the points is more pronounced, with some points having higher errors. These results highlight performance differences between the methods, with MOPC-PC showing more consistent precision, while MOPC-EIS shows greater variability in results. When analyzing the pressure range (15–135 mmHg), both the MOPC-PC and MOPC-EIS methods show different distribution and precision patterns, with MOPC-PC showing greater imprecision than MOPC-EIS in the 15–135 mmHg range. While MOPC-PC has 4 points outside the 5% margin of error, MOPC-EIS has only 2 points outside this margin.

The study developed association functions for the five inputs-aHR, MAP, mF, PA, and PP along with the output flow using 17 fuzzy logic heuristic rules, as outlined by Leao et al. [28]. These functions were implemented as arrays of values, and simplifications of the median calculation based on the centroid of geometric shapes (trapezoids and triangles) and conditional comparison loops were used to calculate the sum of the relevance of the association functions based on their rules. The results of the VAD-MLS test 3 (fuzzy logic) showed that the automatic control by fuzzy logic was comparable on both MOPC-PC and IES architectures for all tested scenarios [37], with the results presented in Table 1 for the comparison of the values obtained by MOPC-PC and IES. This indicates that the implementation of fuzzy logic in IES was equivalent to the original algorithm. The results presented in Table 1 were similar to two decimal places because the fuzzy logic originally developed in Matlab was completely migrated with the same rules and membership functions. Therefore, the expected result of correct execution is similar values for the same inputs in both approaches.

Table 1. Results obtained of the VAD-MLS Test 3: fuzzy logic.

INPUTS					OUTPUT (FLOW)	
aHR	MAP	PA	PP	mF	PC	IES
110	115	0.5	6	5	0.19	0.19
122	74.5	0	4	3.59	0.65	0.65
68.5	117	1	8	5.35	-0.36	-0.36
41.6	148	1	6	0.88	-0.62	-0.62
91.8	106	0	6	2	-0.07	-0.07
64.9	87.5	0	5	2.53	0.2	0.2
80.1	110	1	7	5	-0.2	-0.2
63.1	97.9	1	7	3.94	0.1	0.1
103	74.9	0.5	6	3.94	0.65	0.65
131	97.9	0.5	6	4.88	0.43	0.43
64.9	152	0	6	2.65	-0.43	-0.43
54.2	81.2	0	5	2.65	0.19	0.19
106	131	0.5	5	4.65	-0.03	-0.03
50.6	68.7	0.5	5	6	0.12	0.12
84.6	142	0	3	4.39	-0.26	-0.26

4.2 *Hybrid Cardiovascular Simulator Tests*

Before the HCS test, validation was performed to establish the correlation between practical and estimated values obtained by the IES with integrated MOPC functional modules. The verification was performed through a series of tests on the VAD-MLS with the VAD prototype, using both a flow meter and pressure transducers to measure the flow at various rotational speeds. The results, shown in Figure 6, showed a mean percentage error of $1.2 \pm 0.29\%$ for the flow estimator and $0.67 \pm 0.24\%$ for the differential pressure estimator.

Figure 6 compares the flow and differential pressure estimator values obtained by the Final Estimator of the MOPC-IES with a percentage error within the measurement range of 8 L/min and 150 mmHg, respectively. The Flow Estimator graph in Figure 6 presents 16 data points on the accuracy of the MOPC-IES: (i) the majority of points (15, 93.7%) fall within the 1.5% error range; (ii) 1 point (0.1%) shows errors above 2%; (iii) 8 points (50%) show errors below 1%, with the smallest error close to 0.5%. The Differential Pressure Estimator graph in Figure 6 shows 17 data points for MOPC-IES accuracy: (i) the majority of points (15, 88.2%) fall within the 1.5% error range; (ii) 0 points (0%) show errors above 2%; (iii) 13 points (76.5%) show errors below 1%, with the smallest error close to 0%. The largest errors found were 2.2% for the flow estimator (at 5.1 L/min) and 1.9% for the differential pressure estimator (at 100 mmHg). These errors are well below the previous error range (5%) and close to the current error range (2%), indicating a significant reduction in errors compared to previous findings. As these are special cases, they may be related to in vitro study conditions such as turbulence or noise.
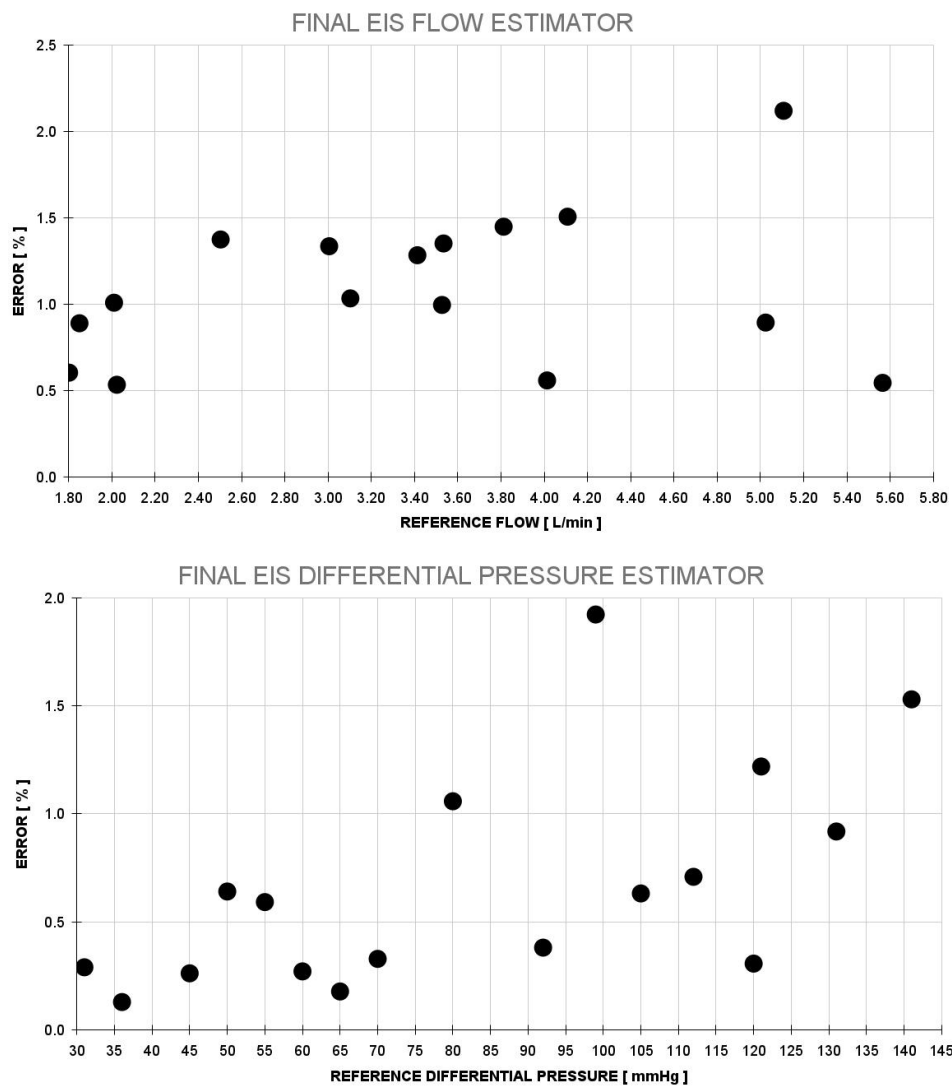
Figure 6. Graph depicting the error relationship between measured data and the reference value for IES with the last version of the flow and differential pressure estimator.

Analysis of the flow range (1.8–5.8 L/min) of the 16 points on the graph shows distinct patterns of percentage error. In the early points, from 1.8 to 3 L/min, the percentage error remains below 1%, indicating relatively high accuracy in this interval. However, as the reference flow increases to about 3 L/min, the percentage error begins to increase and reaches about 1.5%. In the intermediate points, from 3 to 4 L/min, the average percentage errors are higher, between about 1.2% and 1.5%, indicating a lower precision in this interval. Finally, in the last points, from 4 to 5.8 L/min, there is a gradual decrease in the percentage error, dropping to about 1%, which could indicate an improvement in precision as the flow approaches the higher values of the analyzed range; however, the highest error occurs in the range between 5 and 5.2 L/min.

Analysis of the 17 differential pressure points on the graph shows clear trends in the errors observed at different pressure ranges. In the range of 30 to 45 mmHg, the errors remain consistently below 0.5, indicating satisfactory precision in this interval. However, as we move into the range of 50 to 75 mmHg, the errors increase slightly and range between approximately 0.5 and 1, indicating a slight deterioration in accuracy. A more significant increase in error is observed in the range of 80, 100, 120, and 140 mmHg, where the values exceed 1, indicating a lower precision in this interval. However, from 110 to 120 mmHg, the errors begin to decrease again and remain below 1, possibly indicating a partial recovery of precision; however, the highest error value occurs in the 100 mmHg range. Finally, in the range of 130 to 145 mmHg, the error increases again and exceeds 1, indicating a decrease in precision in this higher pressure interval.

Table 2 presents the mean values obtained during the evaluation of the IES in "Closed-loop speed control" mode (HCS Test 1). The parameters assessed include the actual and estimated MAP, CO, HR, SVR, actual and estimated pump flow, and motor speed. The stability of LVAD motor speed control, despite changes in pumping

resistance caused by the physiological system, is demonstrated in Table 2. This indicates the feasibility of the control function provided by the current LVAD controllers available in the market.

Table 2. Results obtained of the IES "Closed-loop speed control" mode in HCS test 1.

LVEF [%]	MAP (Actual) [mmHg]	MAP (Estimated) [mmHg]	CO [L/min]	HR [bpm]	SVR [mmHgs/mL]	Flow (Actual) [L/min]	Flow (Estimated) [L/min]	Speed [rpm]
15	90	95	4.1	80	1.35	4.2	4.27	2500
25	97	96	4.5	80	1.26	4	4.08	2500
35	104	103	5.2	80	1.13	3.2	3.36	2500

Additionally, Table 3 presents the mean values of MAP (actual and estimated), CO, HR, SVR, pump flow (actual and estimated), and motor speed during the evaluation of the IES in "Automatic Speed Control" mode in the recovery of systolic function (HCS Test 2). Table 3 illustrates that the automatic motor speed control of the LVAD responded appropriately to the required assistance, indicating the feasibility of automatic control that synchronizes with the physiological system. This is a capability currently absent in available LVAD controllers.

Table 3. Results obtained of the IES "Automatic Speed Control" mode in HCS test 2.

LVEF [%]	Actual MAP [mmHg]	MAP (Estimated in IES) [mmHg]	CO [L/min]	HR [bpm]	SVR [mmHgs/mL]	Actual flow [L/min]	Flow (Estimated in IES) [L/min]	Speed [rpm]
20	98	95	4.1	80	1.32	4.2	4.25	2400
30	100	101	4.8	80	1.28	4.1	4.03	2300
40	105	103	5.7	80	1.1	3.3	3.5	2000

5. Discussion

This study focuses on the migration of PC-LVAD functionality to an embedded CPS with real-time processing and reconfigurable architecture. Due to their simple algorithms, some PC-LVAD techniques can be integrated into simple microcontroller-based systems. However, most require sophisticated systems with advanced processing capabilities. Some PC LVADs can be implemented using low-cost microcontroller platforms with feedback control algorithms based on a single physiologic variable. Complex systems may require powerful computing platforms such as digital signal processors or FPGAs. The choice of control system platform depends on the specific requirements of the clinical application, including the desired level of control, available computing resources, and cost constraints.

PC-LVADs have been developed with various controllers and monitoring strategies [7]. These strategies can be categorized into four main groups [8]: (i) Preload-based controllers [9,18–23,26]; (ii) Afterload-based controllers [10,12,16,17]; (iii) Heart rate-based controllers [11,12,14,15]; and (iv) Multi-objective controllers [13,24,25,27,28]. Fontana et al. [30] developed a portable system to interface with LVAD sensors and plan to integrate it with the SensorART platform to improve patient quality of life and physician workflow [31]. Fass and Gechter [32] introduced a framework for modeling systems, classifying system dimensions into structural elements, shapes/forms, and dynamics. A PC LVAD was presented within a Health 4.0 framework running on an embedded system [33].

A novel PC-LVAD strategy known as MOPC has been introduced [28]. It is based on the harmonious adaptation of support parameters with the physiological system to optimize the interaction between the LVAD and the patient's body. The MOPC has been successfully validated during in vitro testing, and the next goal for its application as an LVAD control solution is to migrate the concept to an embedded system.

To implement the MOPC in the IES, the original architecture was divided into functional modules, each of which was migrated exclusively to the IES and verified by VAD-MLS results. This approach increased the flexibility of the project, allowing a pause for implementation improvements and the addition of additional modules. After validating each MOPC module on the IES, the entire system was integrated into a unified architecture. Further refinements were made to align the data flow of each control layer. Performance verification under original in vitro validation conditions assessed the success of the MOPC-based architecture, with qualitative analysis based on similarity to previous MOPC results.

First, during the conceptual phase of the controller design, the IES was instantiated on the dedicated PXI® development platform with the 8840 and 7851 modules. Then, during the controller design evaluation phase, the IES was deployed on the MyRIO® development board.

When comparing PXI and MyRIO, several key factors must be considered, including performance, flexibility, cost, and ease of use. In terms of performance, PXI generally offers greater processing power and faster sample rates than MyRIO, due to its modular architecture and ability to utilize high-performance instruments. This makes PXI the preferred choice for applications that require intensive data processing, such as image processing or complex system control. However, PXI's enhanced processing capability and performance typically come at a higher cost, both in terms of hardware and software development. In addition, configuring and managing a PXI system can be more complex than with MyRIO, requiring more technical expertise and implementation time.

On the other hand, MyRIO provides a more affordable and easy-to-use solution for simple to moderately complex applications. Its hardware and software integration streamlines the development process and enables users with less technical experience to create real-time control and monitoring systems quickly and efficiently.

The results shown in Figure 4 indicate that the MOPC-EIS has slightly inferior speed control performance compared to the MOPC-PC. However, the MOPC-EIS exhibits a lower error rate at reference speeds above 40000 rpm. Performance verification under original conditions evaluated the success of the MOPC-based architecture, with analysis based on similarity to previous MOPC results. The speed control in the IES ensured stable operation despite systemic pressure and resistance. The robustness of the system is attributed to the proper calibration of the PI controller. Accurate calibration of PID controllers is critical in dynamic systems such as LVADs [9]. PI control with optimized gains effectively maintains stability and reduces errors in systems requiring rapid response [17]. Studies by Magkoutas et al. [38] examined the influence of gain variation in PID controllers and reported that incorrect settings can lead to undesirable oscillatory responses. Bakouri et al. [39] applied the H-infinity technique, a robust control method, to minimize tracking error and maximize disturbance rejection in LVAD systems. Their approach adjusts pump flow based on metabolic demand using left ventricular end-diastolic volume, with a PI controller maintaining hemodynamic variables within acceptable ranges across different physiological states.

The FPGA-based data acquisition integrated with the RTOS allowed for high motor speed sampling and current data, critical for the IES estimators [28]. Linear LUT interpolation was adopted to optimize FPGA space. The original LUT was expanded to a 32x32 matrix, with non-original values obtained by spline interpolation in MATLAB®. The algorithm was optimized for linear interpolation in the 32x32 LUT, identifying regions of linear value variation. This allowed accurate values to be obtained using exponential and Gaussian formulas, optimizing the space required to implement the estimators in the FPGA system.

In the comparison between the MOPC-PC and MOPC-EIS methods in Figure 5, regarding the accuracy of the flow estimator, both methods show comparable results in terms of precision, with the majority of points falling within the 5% error range. MOPC-EIS shows a slight disadvantage in terms of error values, with one additional point exceeding the 5% error threshold. For the accuracy of the differential pressure estimator, the results of the MOPC-PC and MOPC-EIS are comparable in terms of precision, again with most points within the 5% error range. However, in this case, the MOPC-EIS shows an advantage in accuracy with two fewer points outside the 5% error range and smaller error values, while the MOPC-PC shows a slight tendency to overestimate the flow. The percentage error of the flow estimator was $3.33 \pm 0.92\%$, in agreement with Leao et al. [28] and other estimators [30–42]. The percentage error of the differential pressure estimator was $1.93 \pm 0.7\%$, in agreement with Leao et al. [28] and other estimators. These results confirm the feasibility of using estimators in the IES. It is important to note that the results of the IES control solution were obtained in a virtual environment, while the MOPC operated in the HCS. The calculated mean from Leao et al. [28] indicates the accuracy of the migration. In addition to the estimator migration strategies, refinement techniques were used to improve the estimation process. These include (i) defining the operating range based on the physiological levels of the LVAD to mitigate the adverse effects of motor operation in extreme current and torque ranges, and (ii) creating a variable data collection mesh to construct the LUTs, with more data points in turbulent ranges and fewer in linear operating ranges.

Before the HCS test, a validation was performed to determine the correlation between actual and estimated values obtained by the IES with integrated MOPC modules, as shown in Figure 6. The results showed mean percentage errors of $1.2 \pm 0.29\%$ for flow and $0.67 \pm 0.24\%$ for differential pressure. The analysis showed that the precision varied over different flow ranges, with the highest error observed at 5–5.2 L/min. Similarly,

differential pressure accuracy varied over different pressure ranges, with partial recovery observed in the 110 to 120 mmHg range. A strategy for PC-LVAD with an approach similar to MOPC, incorporating a PI controller based on fuzzy logic to automatically adjust the pump flow, is the study by Bakouri et al. [43], which uses sensorless flow measurements to track a desired reference flow with a dynamic estimator model. In the numerical simulations of this study, the estimator error was significantly lower (within an error margin of 0.25 L/min). This suggests that there is still much research to be done to improve the estimation strategies of the IES. However, on the other hand, in vitro testing presents significantly more complex adversities than those that may be encountered in a virtual environment. Therefore, the error obtained in the proposal of this study can be considered satisfactory considering the specialized literature in this field [30–42]. Nevertheless, in vivo testing also presents even higher levels of complexity that cannot be replicated in an in vitro study, and new studies under these conditions will always be necessary. On the other hand, although estimators are commonly used in control systems, their suitability for clinical use may be questionable. In a recent study [44], the IES was used to implement and compare the performance of a sensor-based feedback controller. The strategies were tested on a simulated systemic circulation, and the results showed that the use of pressure sensors resulted in a more accurate controller response compared to the use of estimators. These results underscore the importance of careful consideration of measurement technologies when designing control systems for clinical applications.

In the HCS tests, the behavior of the MOPC within the IES demonstrated a satisfactory perception of the evolution of the patient's clinical condition. This was evidenced by the ability to increase flow when the patient was heavily dependent on the LVAD and to decrease flow when the patient was recovering, as shown in Table 3. Adjustment was accomplished without compromising MAP and preventing backflow through the pump. The active baroreflex system in the HCS tests underscores the importance of the results in harmonious interaction with the physiological circulatory regulatory system. These findings need to be validated and further investigated for overperfusion and ventricular collapse in both MLS tests and HCS results in future research. Confirmation by in vivo experiments is necessary to establish their clinical applicability. Meanwhile, Santos & Cestari [45] present a computational simulator to further explore the intricacies of PC-LVAD functionality. This simulator evaluates hemodynamic responses in different scenarios, facilitating a comparison of PC-LVAD operations. Santos & Cestari [45] extend this investigation by integrating simulations of patient conditions, mathematical models of estimators and sensors, and PC-LVAD algorithms. These research efforts represent significant progress in understanding and improving the effectiveness of these control strategies in the preclinical setting.

Long-term LVAD therapy aims to prevent ventricular suction during changes in vascular resistance. The PC-LVAD requires increased preload and decreased afterload sensitivity. The MOPC was designed with anti-suction rules. The IES solution could include a module for dedicated anti-suction control and real-time alerts that empower the patient and allow the clinician to adjust treatment. The IES could be enhanced by incorporating AI modules, using data from estimators and sensors, or improving automatic control settings. The goal is to accelerate diagnosis, tailor treatments, reduce medical costs, and transition from periodic intervention to continuous monitoring and personalized treatment.

This study explores a feasible controller for the physiological regulation of LVADs and provides valuable insights that could advance the field. However, it has limitations. The IES is a proof of concept for a real-time embedded LVAD, but it is not ready for medical use. Results from bench testing, where a controller activates a prototype LVAD, have limitations and do not fully capture the complexity of clinical use.

6. Conclusion

This study makes a significant contribution to the development of LVAD controllers. By introducing an innovative approach to incorporate a CPS into the LVAD controller design, the article expands the functionality of the device and opens new possibilities for control and monitoring. The proposed modular architecture divides the original LVAD controller into functional modules that are migrated to the IES, allowing for easier maintenance, scalability, and system adaptability. Validation of the multiobjective-based architecture ensured the reliability and effectiveness of the proposed embedded system. The emphasis on stable operation, accurate estimation, and adaptive refinement techniques highlights the importance of symmetry in the LVAD system, contributing to improved patient outcomes and device reliability. Successful control and calibration of estimator parameters demonstrate a symmetric relationship between computational management and physical response,

ensuring accurate and reliable LVAD operation. The application of flow and differential pressure measurement estimators is shown to be feasible, improving data accuracy collection and LVAD system monitoring. In addition, the migration of the fuzzy logic-based expert system from the MPC enables automatic control, allowing the LVAD to respond effectively to changes in the patient's clinical profile during testing. Future studies should prioritize the evaluation of the clinical benefits and risks of implementing the PC-LVAD-embedded CPS.

Acknowledgments

Conflict of Interest

There is no conflict of interest for this study.

References

[1] Lilly, L.S. *Braunwald's Heart Disease Review and Assessment E-Book: A Companion to Braunwald's Heart Disease*. Elsevier Health Sciences: Amsterdam, Netherlands, 2022.

[2] Mantha, A.; Lee, R.O.J.; Wolfson, A.M. Patient selection for heart transplant: balancing risk. *Curr. Opin. Organ Transplant.* **2021**, *27*, 36–44, https://doi.org/10.1097/mot.0000000000000943.

[3] Berardi, C.; Bravo, C.A.; Li, S.; Khorsandi, M.; Keenan, J.E.; Auld, J.; Rockom, S.; Beckman, J.A.; Mahr, C. The History of Durable Left Ventricular Assist Devices and Comparison of Outcomes: HeartWare, HeartMate II, HeartMate 3, and the Future of Mechanical Circulatory Support. *J. Clin. Med.* **2022**, *11*, 2022, https://doi.org/10.3390/jcm11072022.

[4] Yuzefpolskaya, M.; Schroeder, S.E.; Houston, B.A.; Robinson, M.R.; Gosev, I.; Reyentovich, A.; Koehl, D.; Cantor, R.; Jorde, U.P.; Kirklin, J.K.; et al. The Society of Thoracic Surgeons Intermacs 2022 Annual Report: Focus on the 2018 Heart Transplant Allocation System. *Ann. Thorac. Surg.* **2022**, *115*, 311–327, https://doi.org/10.1016/j.athoracsur.2022.11.023.

[5] Stephens, A.F.; Gregory, S.D.; Burrell, A.J.; Marasco, S.; Stub, D.; Salamonsen, R.F. Physiological principles of Starling-like control of rotary ventricular assist devices. *Expert Rev. Med Devices* **2020**, *17*, 1169–1182, https://doi.org/10.1080/17434440.2020.1841631.

[6] Tchantchaleishvili, V.; Luc, J.G.Y.; Cohan, C.M.; Phan, K.; Hübbert, L.; Day, S.W.; Massey, H.T. Clinical Implications of Physiologic Flow Adjustment in Continuous-Flow Left Ventricular Assist Devices. *ASAIO J.* **2017**, *63*, 241–250, https://doi.org/10.1097/mat.0000000000000477.

[7] Santos, B.; Leão, T. Control Systems. In *Bioengineering and Biomaterials in Ventricular Assist Devices,* CRC Press: Boca Raton, FL, USA, 2021; pp 75–109, https://doi.org/10.1201/9781003138358-5.

[8] Ochsner, G.; Amacher, R.; Wilhelm, M.J.; Vandenberghe, S.; Tevaearai, H.; Plass, A.; Amstutz, A.; Falk, V.; Daners, M.S. A Physiological Controller for Turbodynamic Ventricular Assist Devices Based on a Measurement of the Left Ventricular Volume. *Artif. Organs* **2013**, *38*, 527–538, https://doi.org/10.1111/aor.12225.

[9] Endo, G.; Araki, K.; Oshikawa, M.; Kojima, K.; Saitoh, T.; Nakamura, K.; Onitsuka, T. Control Strategy for Biventricular Assistance with Mixed-Flow Pumps. *Artif. Organs* **2000**, *24*, 594–599, https://doi.org/10.1046/j.1525-1594.2000.06589.x.

[10] Waters, T.; Allaire, P.; Tao, G.; Adams, M.; Bearnson, G.; Wei, N.; Hilton, E.; Baloh, M.; Olsen, D.; Khanwilkar, P. Motor Feedback Physiological Control for a Continuous Flow Ventricular Assist Device. *Artif. Organs* **1999**, *23*, 480–486, https://doi.org/10.1046/j.1525-1594.1999.06386.x.

[11] Ohuchi, K.; Kikugawa, D.; Takahashi, K.; Uemura, M.; Nakamura, M.; Murakami, T.; Sakamoto, T.; Takatani, S. Control Strategy for Rotary Blood Pumps. *Artif. Organs* **2001**, *25*, 366–370, https://doi.org/10.1046/j.1525-1594.2001.025005366.x.

[12] Bullister, E.; Reich, S.; Sluetz, J. Physiologic Control Algorithms for Rotary Blood Pumps Using Pressure Sensor Input. *Artif. Organs* **2002**, *26*, 931–938, https://doi.org/10.1046/j.1525-1594.2002.07126.x.

[13] Boston, J.; Antaki, J.; Simaan, M. The development of control techniques for ventricular-assist devices and a hierarchical control structure to regulate the operation of a turbo-hydrodynamic assist device - Hierarchical control of heart-assist devices. *IEEE Robot. Autom. Mag.* **2003**, *10*, 54–64, https://doi.org/10.1109/mra.2003.1191711.

[14] Vollkron, M.; Schima, H.; Huber, L.; Benkowski, R.; Morello, G.; Wieselthaler, G. Development of a Reliable Automatic Speed Control System for Rotary Blood Pumps. *J. Hear. Lung Transplant.* **2005**, *24*, 1878–1885, https://doi.org/10.1016/j.healun.2005.02.004.

[15] Schima, H.; Vollkron, M.; Jantsch, U.; Crevenna, R.; Roethy, W.; Benkowski, R.; Morello, G.; Quittan, M.; Hiesmayr, M.; Wieselthaler, G. First Clinical Experience with an Automatic Control System for Rotary Blood Pumps During Ergometry and Right-Heart Catheterization. *J. Hear. Lung Transplant.* **2006**, *25*, 167–173, https://doi.org/10.1016/j.healun.2005.09.008.

[16] Giridharan, G.A.; Skliar, M. Physiological Control of Blood Pumps Using Intrinsic Pump Parameters: A Computer Simulation Study. *Artif. Organs* **2006**, *30*, 301–307, https://doi.org/10.1111/j.1525-1594.2006.00217.x.

[17] Wu, Y.; Allaire, P.E.; Tao, G.; Olsen, D. Modeling, Estimation, and Control of Human Circulatory System With a Left Ventricular Assist Device. *IEEE Trans. Control. Syst. Technol.* **2007**, *15*, 754–767, https://doi.org/10.1109/tcst.2006.890288.

[18] Choi, S.; Antaki, J.; Boston, R.; Thomas, D. A sensorless approach to control of a turbodynamic left ventricular assist system. *IEEE Trans. Control. Syst. Technol.* **2001**, *9*, 473–482, https://doi.org/10.1109/87.918900.

[19] Gwak, K.-W. Application of Extremum Seeking Control to Turbodynamic Blood Pumps. *ASAIO J.* **2007**, *53*, 403–409, https://doi.org/10.1097/mat.0b013e31806ada0a.

[20] Arndt, A.; Nüsser, P.; Graichen, K.; Müller, J.; Lampe, B. Physiological Control of a Rotary Blood Pump With Selectable Therapeutic Options: Control of Pulsatility Gradient. *Artif. Organs* **2008**, *32*, 761–771, https://doi.org/10.1111/j.1525-1594.2008.00628.x.

[21] Stevens, M.C.; Wilson, S.; Bradley, A.; Fraser, J.; Timms, D. Physiological Control of Dual Rotary Pumps as a Biventricular Assist Device Using a Master/Slave Approach. *Artif. Organs* **2014**, *38*, 766–774, https://doi.org/10.1111/aor.12303.

[22] Stephens, A.F.; Stevens, M.C.; Gregory, S.D.; Kleinheyer, M.; Salamonsen, R.F. In Vitro Evaluation of an Immediate Response Starling-Like Controller for Dual Rotary Blood Pumps. *Artif. Organs* **2017**, *41*, 911–922, https://doi.org/10.1111/aor.12962.

[23] Cysyk, J.; Jhun, C.-S.; Newswanger, R.; Weiss, W.; Rosenberg, G. Rotary blood pump control using integrated inlet pressure sensor. In Proceedings of 2011 Annual International Conference of the IEEE Engineering in Medicine and Biology Society, Boston, MA, USA, 30 August–3 September 2011, https://doi.org/10.1109/IEMBS.2011.6090121.

[24] Cysyk, J.; Jhun, C.-S.; Newswanger, R.; Pae, W.; Izer, J.; Flory, H.; Reibson, J.; Weiss, W.; Rosenberg, G. In Vivo Evaluation of a Physiologic Control System for Rotary Blood Pumps Based on the Left Ventricular Pressure-Volume Loop. *ASAIO J.* **2021**, *68*, 791–799, https://doi.org/10.1097/mat.0000000000001619.

[25] Petrou, A.; Ochsner, G.; Amacher, R.; Pergantis, P.; Rebholz, M.; Meboldt, M.; Daners, M.S. A Physiological Controller for Turbodynamic Ventricular Assist Devices Based on Left Ventricular Systolic Pressure. *Artif. Organs* **2016**, *40*, 842–855, https://doi.org/10.1111/aor.12820.

[26] Petrou, A.; Monn, M.; Meboldt, M.; Daners, M.S. A Novel Multi-objective Physiological Control System for Rotary Left Ventricular Assist Devices. *Ann. Biomed. Eng.* **2017**, *45*, 2899–2910, https://doi.org/10.1007/s10439-017-1919-0.

[27] Fetanat, M.; Stevens, M.; Hayward, C.; Lovell, N.H. A Sensorless Control System for an Implantable Heart Pump Using a Real-Time Deep Convolutional Neural Network. *IEEE Trans. Biomed. Eng.* **2021**, *68*, 3029–3038, https://doi.org/10.1109/tbme.2021.3061405.

[28] Leao, T.; Utiyama, B.; Fonseca, J.; Bock, E.; Andrade, A. In vitro evaluation of multi-objective physiological control of the centrifugal blood pump. *Artif. Organs* **2020**, *44*, 785–796, https://doi.org/10.1111/aor.13639.

[29] Pauls, J.P.; Stevens, M.C.; Bartnikowski, N.; Fraser, J.F.; Gregory, S.D.; Tansley, G. Evaluation of Physiological Control Systems for Rotary Left Ventricular Assist Devices: An In-Vitro Study. *Ann. Biomed. Eng.* **2016**, *44*, 2377–2387, https://doi.org/10.1007/s10439-016-1552-3.

[30] Fontana, R.; Tortora, G.; Silvestri, M.; Vatteroni, M.; Dario, P.; Trivella, M. A portable system for autoregulation and wireless control of sensorized left ventricular assist devices. *Biocybern. Biomed. Eng.* **2016**, *36*, 366–374, https://doi.org/10.1016/j.bbe.2016.02.001.

[31] Verbeni, A.; Fontana, R.; Silvestri, M.; Tortora, G.; Vatteroni, M.; Trivella, M.G.; Dario, P. An Innovative Adaptive Control Strategy for Sensorized Left Ventricular Assist Devices. *IEEE Trans. Biomed. Circuits Syst.* **2014**, *8*, 660–668, https://doi.org/10.1109/tbcas.2014.2346015.

[32] Fass, D.; Gechter, F. Towards a theory for bio-cyber physical systems modelling. In *Digital Human Modeling. Applications in Health, Safety, Ergonomics and Risk Management: Human Modeling*, Springer: Cham, Switzerland, 2015; pp 245–255, https://doi.org/10.1007/978-3-319-21073-5_25.

[33] Santos, B.; Barboza, M.; Leão, T.; Santos, D.; Andrade, A.; Bock, E. Intelligent embedded system for physiological control of ventricular assist devices in health 4.0 Background. *Int. J. Adv. Med Biotechnol. - IJAMB* **2023**, *5*, https://doi.org/10.52466/ijamb.v5i2.112.

[34] Santos, B.; Leão, T.; Drigo, E.; Fonseca, J.; Andrade, A.; Nishida, B.; Bock, E. Design of a Hydrodynamic Performance Bench for Ventricular Assist Devices. *Acad. Soc. J.* **2022**, *6*, 7–26, https://doi.org/10.32640/tasj.2022.1.7.

[35] da Silva, B.U.; da Fonseca, J.W.G.; Leal, E.B.; Cardoso, J.R.; Biscegli, J.F.; de Andrade, A.J.P. Apical aortic blood pump preclinical assessment for long-term use: Durability test and stator topology to reduce wear in the bearing system. *Artif. Organs* **2019**, *44*, 779–784, https://doi.org/10.1111/aor.13587.

[36] Fonseca, J.; Andrade, A.; Nicolosi, D.E.; Biscegli, J.F.; Leme, J.; Legendre, D.; Bock, E.; Lucchi, J.C. Cardiovascular Simulator Improvement: Pressure Versus Volume Loop Assessment. *Artif. Organs* **2011**, *35*, 454–458, https://doi.org/10.1111/j.1525-1594.2011.01266.x.

[37] Santos, B.; Leão, T.; Bock, E. Intelligent Control based on Fuzzy logic embedded in FPGA applied in Ventricular Assist Devices (VADs). In Proceedings of the 2019 4th International Conference on Robotics, Control and Automation, Guangzhou, China, 26–28 July 2019, https://doi.org/10.1145/3351180.3351198.

[38] Magkoutas, K.; Rossato, L.N.; Heim, M.; Daners, M.S. Genetic algorithm-based optimization framework for control parameters of ventricular assist devices. *Biomed. Signal Process. Control.* **2023**, *85*, https://doi.org/10.1016/j.bspc.2023.104788.

[39] Bakouri, M.; Alassaf, A.; Alshareef, K.; Abdelsalam, S.; Ismail, H.F.; Ganoun, A.; Alomari, A.-H. An Optimal H-Infinity Controller for Left Ventricular Assist Devices Based on a Starling-like Controller: A Simulation Study. *Mathematics* **2022**, *10*, 731, https://doi.org/10.3390/math10050731.

[40] Tsukiya, T.; Taenaka, Y.; Nishinaka, T.; Oshikawa, M.; Ohnishi, H.; Tatsumi, E.; Takano, H.; Konishi, Y.; Ito, K.; Shimada, M. Application of Indirect Flow Rate Measurement Using Motor Driving Signals to a Centrifugal Blood Pump with an Integrated Motor. *Artif. Organs* **2001**, *25*, 692–696, https://doi.org/10.1046/j.1525-1594.2001.06858.x.

[41] Tanaka, A.; Yoshizawa, M.; Abe, K.; Takeda, H.; Yambe, T.; Nitta, S. In Vivo Test of Pressure Head and Flow Rate Estimation in a Continuous-Flow Artificial Heart. *Artif. Organs* **2003**, *27*, 99–103, https://doi.org/10.1046/j.1525-1594.2003.07175.x.

[42] Zhang, X.T.; AlOmari, A.H.; Savkin, A.V.; Ayre, P.J.; Lim, E.; Salamonsen, R.F.; Rosenfeldt, F.L.; Lovell, N.H. In vivo validation of pulsatile flow and differential pressure estimation models in a left ventricular assist device. In Proceedings of 2010 32nd Annual International Conference of the IEEE Engineering in Medicine and Biology Society (EMBC 2010), Buenos Aires, Argentina, 31 August–4 September 2010, https://doi.org/10.1109/IEMBS.2010.5626876.

[43] Bakouri, M.; Alassaf, A.; Alshareef, K.; AlMohimeed, I.; Alqahtani, A.; Aboamer, M.A.; Alonazi, K.A.; Alharbi, Y. In Silico Evaluation of a Physiological Controller for a Rotary Blood Pump Based on a Sensorless Estimator. *Appl. Sci.* **2022**, *12*, 11537, https://doi.org/10.3390/app122211537.

[44] Santos, B.; Cestari, I. A Multi-objective Physiological Control for Continuous Flow Left Ventricular Assist Devices: Comparison of Estimator versus Sensor-based Feedback*. In proceedings of 2023 45th Annual International Conference of the IEEE Engineering in Medicine & Biology Society (EMBC), Sydney, Australia, 24–27 July 2023, https://doi.org/10.1109/EMBC40787.2023.1034097.

[45] Santos, B. J.; Cestari, I. A. Development of a Computational Simulator of the Physiological Control of Ventricular Assist Devices (VADs). In *IX Latin American Congress on Biomedical Engineering and XXVIII Brazilian Congress on Biomedical Engineering*, Springer: Cham, Switzerland, 2024; pp 454–461, https://doi.org/10.1007/978-3-031-49401-7_47.